Materials Horizons

ROYAL SOCIETY OF CHEMISTRY

COMMUNICATION

View Article Online
View Journal | View Issue

Cite this: *Mater. Horiz.*, 2020, 7, 1888

Received 4th March 2020,
Accepted 16th April 2020

DOI: 10.1039/d0mh00385a

rsc.li/materials-horizons

Temperature dependence of the spectral line-width of charge-transfer state emission in organic solar cells; static *vs.* dynamic disorder†

Kristofer Tvingstedt, *[a] Johannes Benduhn [b] and Koen Vandewal [c]

The origin of energetic disorder in organic semiconductors and its impact on opto-electronic properties remains a topic of intense controversy. Particularly the disorder at electron donor–acceptor interfaces for organic photovoltaics is pivotal to understand as it is expected to affect photo-carrier generation, recombination and consequently device efficiency parameters. In this work we evaluate the temperature dependence of the line-shape of the photo-luminescence (PL) and electroluminescence (EL) spectra of small molecule:fullerene blend devices, with the ambition to disentangle dynamic and static disorder contributions. The EL emission spectra are dominated by charge-transfer (CT) state emission and are confirmed to be of Gaussian character and almost completely voltage independent. More importantly, a strong line-width narrowing is persistently observed upon cooling, down to a certain material specific low temperature, below which the line-width remains constant. It is consequently clear that the main portion of the line-width measured at operating conditions of room temperature or higher, is originating from thermally activated, or dynamic, disorder. The observed temperature dependence of the high-energy emission tail can be fully described by taking into account high and low frequency molecular vibrational modes, without having to rely on static disorder. The presence of low frequency molecular modes with large Huang–Rhys factors results in a Gaussian line-shape, which is additionally broadened at high temperature by thermal population of high frequency intra-molecular modes. We therefore cast strong doubts regarding the commonly used assumption that single temperature optical measurements of absorption or emission tails are able to provide meaningful information regarding the shape of a static density of states tail.

New concepts

Absorption and emission tails of semiconducting materials are often considered a probe of energetic disorder. For photovoltaic materials, a broad energetic distribution of the density of states limits both open-circuit voltage and charge transport properties. In organic semiconductors and their blends, the origin of absorption and emission tails and their relation to the density of states is however still unclear. As the high-energy emission tail is often easier to measure than the absorption tail, we here perform a highly sensitive study of the temperature dependence of the emission spectra of a multitude of organic solar cells. Our main ambition is to explain and disentangle the contribution from static disorder (inhomogeneous) and vibrational (dynamic or homogeneous) broadening. Our measured emission spectra are dominated by charge-transfer-state emission, and we persistently observe a pronounced line-width narrowing upon cooling, down to a certain material specific low temperature below which the line-width remains constant. We rationalize these experimental observations with a Franck–Condon vibrational picture without having to account for any contribution from static disorder. We therefore also cast strong doubts regarding the now commonly used assumption that single temperature optical measurements provides meaningful information regarding the shape of a static density of states tail.

1. Introduction

Charge carrier generation and recombination at donor–acceptor interfaces in organic solar cells (OPVs) are now well known to involve charge-transfer states. These intermolecular electronic states have been quite well characterized and are recognized to lead to additional weak absorption and emission features below the optical gaps of the individual donor and acceptor material constituting the blend. However, a pronounced riddle lies unresolved on the correct assignment of the true origin of the width of the absorption tail and the, by reciprocity relations related,[1] corresponding spectral line-width of the high-energy emission tail. Broad low-energy absorption tails and consequently broad high-energy tails in the emission spectra, as well as large Stokes shifts, are always undesired properties for a solar cell to possess, as they are a sign of a large energetic disorder, detrimental for charge transport, recombination and open-circuit voltage. However, the microscopic origin of the

[a] *Experimental Physics VI, Julius-Maximilian University of Würzburg, Am Hubland, 97074 Würzburg, Germany. E-mail: ktvingstedt@physik.uni-wuerzburg.de*
[b] *Dresden Integrated Center for Applied Physics and Photonic Materials (IAPP) and Institute for Applied Physics, Technische Universität Dresden, Nöthnitzer Str. 61, 01187 Dresden, Germany*
[c] *Institute for Materials Research (IMO-IMOMEC), Hasselt University, Wetenschapspark 1, 3590 Diepenbeek, Belgium*

† Electronic supplementary information (ESI) available. See DOI: 10.1039/d0mh00385a

absorption- and emission-tails in most solar cells, including OPVs, is actually not clear. Earlier measurements and models on a multitude of different materials have often demonstrated exponential absorption tails with slopes usually referred to as the Urbach edge with an associated Urbach energy ($E_U(T)$) or Urbach slope (σ_U). Such tails are fitted by the following expression:

$$\alpha(E,T) = \alpha_0 e^{-\frac{(E_0-E)}{E_U(T)}} = \alpha_0 e^{-\frac{\sigma_U(E_0-E)}{kT}} \quad (1)$$

The origin and appropriate description of exponential absorption edges following Urbach's rule (eqn (1)) has been discussed heavily during the last 60 years.[2] It was argued that the observation of exponential absorption tails could be attributed to impurities[3] or correspondingly to the exponential tail shape[4] of the density of states (DOS). The absorption tail was also demonstrated to correlate with compositional variations of the constituting materials in compound semiconductors, both for GeSe[5] and hydrogenated amorphous silicon.[6] The width of the absorption tail and the corresponding emission line-width are in these papers mostly ruled by the convolution of the energetic distribution of the impurity-broadened DOS for electrons and holes, and are therefore essentially a static and temperature independent property. However, the original description by Urbach,[7] was very clear in its temperature dependence, with the broadened slopes described as exclusively thermally activated dynamic processes (Rightmost expression in eqn (1)). A significant amount of the discussion on the true origins of the Urbach tail has since then been regularly centered on whether the slopes are generally ruled by temperature-activated processes (strong phonon coupling) or if it is instead originating from the static structural disorder of the material. The consensus reached within the inorganic and ionic crystal research field has matured into that the tail broadening of amorphous materials (such as hydrogenated amorphous Si) are typically ruled by static structural disorder, whereas tail broadening of purer crystals (such as crystalline Si and the early ionic crystals studied in the original work by Urbach) is instead mostly governed by dynamic disorder, as a result of thermally induced vibrations of the lattice. Structural (static) and thermal (dynamic) disorder as determined from Urbach tails has later been concluded[2,6] to be additive, where both GaAs[8] as well as crystalline[8] and amorphous[6] Si, and a multitude of other ionic crystals have also been assigned as having both a dynamic and static contribution to the total Urbach tail:

$$E_U(T) = E_U^{stat}(0) + E_U^{dyn}(T) \quad (2)$$

In line with the earlier models for amorphous inorganic semiconductors, later work concludes that also for organic semiconductors and their blends, energetic disorder, described by either an exponential (with associated E_U), but more often a Gaussian (with variance σ_{Gauss}) DOS, must be accounted for in the description of optical transition tails.[9]

A direct consequence of purely static localized exponential tail state distribution is that the EL emission peak must[10,11] display a pronounced voltage dependence, as a direct consequence of the fact that upon increasing carrier concentration, higher localized energy states within the exponential DOS are filled. However, Gong *et al.*[12] showed that this did not really seem to be the case for a majority of OPV cells evaluated. Hörmann *et al.* recently showed noticeable bias dependent EL peak shifts in metaloxide:organic solar cells, and has argued that its origin could both be due to tail state filling[13] but could also be assigned to a Stark effect[14] (internal field dependence of polarizable molecules).

Contrary to a picture where static disorder dominates, we suggested earlier[15] that the absorption tail and the corresponding emission line-width of organic solar cells can be quite well described in the framework of classical molecular Marcus theory. In this picture, the observed (often Gaussian) spectral shape of both the emission and the absorption tails are instead exclusively described by a reorganization energy (λ) associated with the interfacial charge-transfer state. Instead of absorption/emission being ruled by the temperature independent shape (tail) of a static DOS, optical transitions are in this model determined only by the vibrational wave-function overlap between thermally populated vibrational ground/excited state levels and any vibrational excited/ground state level, respectively. This type of broadening related to vibrations is therefore referred to as dynamic disorder broadening.

Fig. 1 outlines a sketch of the two extreme cases of pure static disorder and pure dynamic disorder of charge-transfer excitons at the interface between donor and acceptor molecules. In general, both static and dynamic contributions to the total absorption tail and the emission line-width are to be expected, and combinations of the two cases in Fig. 1 should hence be anticipated. If a static Gaussian disorder is described simply by a temperature independent energetic variance σ_S and the dynamic disorder parameter described by a temperature dependent $\sigma_D(T)$, the sum of these two simultaneous contributions add up to the total variance σ_T quadratically:

$$\sigma_T^2(T) = \sigma_S^2 + \sigma_D^2(T) \quad (3)$$

As a multitude of material properties rules the probabilities for optical transitions, it is in principle not possible to uniquely determine neither the shape of the DOS nor the transition-matrix element from absorption and emission tails measured

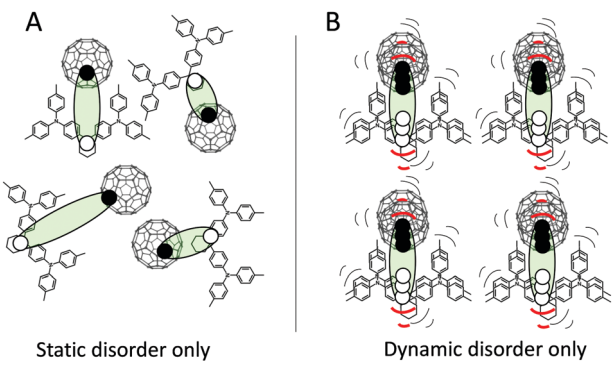

Fig. 1 TAPC and C_{60} with the CT excitons sketched with filled circles = electrons and open circles = holes. Panel (A) outlines the example of static disorder, where different energies are existing due to different spatial configurations. (B) shows instead an ordered spatial set of molecules that, in contrast to panel (A), are strongly vibrating and hence symbolizes the dynamic disorder case.

just at room temperature. Yet, in early amorphous Si literature, it has for example been assumed that the matrix element is constant and that the DOS shape could be straightforwardly determined[4,16] from single temperature tail spectral measurements. The same assumption has also been made in organic photovoltaic materials.[9] In contrast, the classical Marcus model[17,18] that we originally employed,[19,20] does not account for any static disorder contribution but confides solely on the dynamic contribution, whose variance is defined by:[19,21]

$$\sigma_D^2(T) = 2\lambda kT \quad (4)$$

A consequence of this assumption is that the Gaussian variance associated with the spectral line-width is expected to show a direct linear relationship with temperature, although this was never experimentally proven. A mathematical concern of the classical Marcus picture is that it also predicts a vanishingly small transfer rate and emission line-width at very low temperatures, which indeed seems quite unreasonable. What is here however particularly important to bear in mind is that the Marcus theory embodies only a classical approximation valid in the high temperature regime where the thermal energy of the system is assumed to be larger than the relevant vibrational energy spacings ($kT > \hbar\omega$) of the system. The regular C–C vibrational modes in organics have $\hbar\omega$ of around 150 meV, thus substantially exceeding kT even at operational temperatures, clearly violating the requirement for the classical approximation. However, it is important to recognize that there are also a whole range of much lower frequency modes present, related to the movement of entire molecules or vibrations of large fractions of the molecules and their surroundings.[22,23] It is still quite unclear how the occurrence of both high and low frequency modes generally affects the absorption and emission tails and their temperature dependence in organic solar cells.

First attempts to disentangle the contributions of σ_S and σ_D were presented in the work of Burke *et al.*,[21] who found that the CT-state absorption tail of regio-random P3HT:PCBM could be described using a $\sigma_S \approx 104$ meV and a σ_D of 48 meV at 300 K. Further recent analysis of EQE tails combined with theoretical work suggested[23] on the contrary that the contribution from static disorder however did not appear to constitute a major part of the tail width in small molecule:C_{60} samples. It was also concluded from DFT simulations that low frequency intramolecular vibrations on donor and acceptor molecules are the main contributors to the CT-state absorption tails. Very recently, Kahle *et al.*[24] however questioned this description and pointed out that a complete quantum mechanical Frank–Condon (F–C) picture (or Levitch–Jortner formalism[25]) should be employed, taking into account both low and high frequency vibrations. In line with Burke's EQE measurements, the static temperature independent energetic disorder of their studied system (MeLPPP:PCBM60) was also concluded to dominate the spectral line-width of emission. As only weak alteration of the CT emission spectra was observed over a large temperature range, the assigned energetic disorder amounted to $\sigma_S = 67$ meV and the 300 K dynamic disorder $\sigma_D = 45$ meV. This renders the static line-width contribution according to eqn (3) more than twice that of the dynamic 300 K contribution. We notice that the general temperature independence of their measured CT emission line-width seems to be in accordance with previous PL CT measurements by Jarzab[26] on PCPDTBT:PCBM, but in strong contrast to the work by Riisnes[27] on F8T2:PCBM. Along with Burke *et al.*, it was thus strongly emphasized that the contribution from static energetic disorder (inhomogeneous broadening) should not be neglected. Although we fully agree with the interpretations made, and the need of a complete F–C model, we will here demonstrate for a series of small molecule: fullerene and polymer:fullerene samples that the relative contributions of σ_S and σ_D as determined from optical measurements, does not really appear to be represented by the results provided by neither Kahle *et al.*,[24] Street *et al.*[9] nor Burke *et al.*[21]

As the energetic distribution of the emission is reciprocal with the absorption tail, it allows straightforward access to the relevant properties ruling the sought-after optical transitions. Herein we will therefore focus our study on (intermolecular) CT-state emission and show, for a multitude of different organic bulk heterojunction PV systems that the dominant part of the spectral line-width does in fact not appear to be subjugated to static energetic disorder. We instead find a clearly temperature dependent emission line-width defined by vibrational modes of the bulk heterojunction molecules. We first show that our T dependent observations can be quite well described by a system governed by low energy vibrations (<20 meV). A more complete description however requires a full quantum mechanical treatment that accounts also for combinations of both low and high-energy vibrational modes. Our results therefore cast strong doubt on the common practice to extract a static DOS from optical tail measurements.

2. Results

Before presenting experimental results and interpreting temperature dependent emission spectral measurements, we want to make a note on the effect of thin film optical interference. As recently pointed out by List *et al.*,[28] thin film optical interference effects lead to a wavelength dependent light outcoupling efficiency, which can disrupt the spectral shape as well as the peak position of emission, complicating the assignment of the sought after dependence of internal energetic transitions. The absolute values of peak positions as well as line-widths are thus expected to be slightly inaccurate according to the vindicated claims by List *et al.*, but, as optical interference and outcoupling efficiency is not expected to be temperature dependent, the overall measured and presented temperature-dependence in this work is expected to preserve the true behaviour of the internal transitions. Although we cannot fully rule out the combined effect of EL emission-zone shifts and potential altered out-coupling efficiency with temperature, we deem the voltage independence of the spectra from devices and the overall similar behavior of the EL spectra of devices and PL spectra of films (*vide infra*) a strong gauge against this effect.

We start by a brief recapitulation of charge-transfer state emission in relation to the excitonic emission of the pure organic

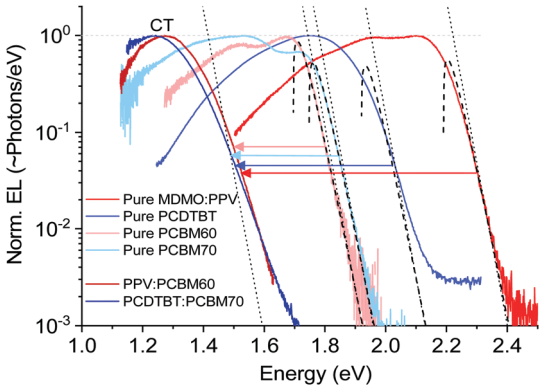

Fig. 2 Normalized electroluminescence spectra of some classical pure OPV materials and blends on logarithmic scale, emphasizing the varying slope of the high-energy tail. Dashed lines are fits to the well-known relation in eqn (5), whereas the dotted lines are accounting only for the exponential part of the same equation.

material constituents in OPV blends. Fig. 2 shows an archetypal example of the relationship between the emission of two OPV blends and the two materials constituting these blends, in this case the prior OPV working horses MDMO-PPV:PCBM60 and PCDTBT:PCBM70. In line with a majority of other (later and better) OPV cells, the pure acceptor peaks are redshifted with respect to the pure donors, and the CT-state peaks (from the blends) are further redshifted into the NIR region.

The important feature worth highlighting in Fig. 2 is the overall slope of the high-energy tail of the emission peaks, which represents the main studied parameter of this work. Three of the pure materials all show quite steep slopes that can be fairly well approximated by a simple exponential function over more than two decades of measured data. The exponential shape is here fitted by a simple Boltzmann population of a three dimensional square-root shaped DOS whose band to band distribution of high energy emission is regularly given by:[29,30]

$$R(E) = A \cdot E \cdot (E - E_G)^{\frac{1}{2}} \cdot e^{-\frac{E}{kT}} \quad (5)$$

In this expression, often used to determine the junction temperature of direct bandgap solid-state inorganic diodes, broadening due to both disorder and phonon-interaction is neglected and the main parameter that defines the slope is the temperature of the device. This neglection however seems to work surprisingly fine for the two fullerenes, fails modestly for the pure PPV and PCDTBT and obviously fails completely for the two presented CT-state peaks. The fits in the graphs all employ T = 300 K and an E_G of 1.70 eV, 1.75 eV, 1.92 eV and 2.19 eV for PCBM60, PCBM70, PCDTBT and the PPV respectively. The high-energy tail of the CT-state spectra can obviously not be described by exponential functions, but, as outlined previously, is instead often better represented by a broad Gaussian distribution.

2.1. Temperature dependence of neat C_{60} photoluminescence

As a counterexample to the thermal behavior of interfacial CT-state line-widths, we proceed by showing the highly structured spectra of pure C_{60}, demonstrating archetypal and assignable high-energy (intra-molecular) organic vibronic progressions. The pure Buckminster fullerene molecule has been intensively studied since it was first[31] observed. A plethora of prior studies[32–35] has already dealt with the assignment of its temperature dependent spectral features, although the conclusions have varied somewhat throughout the decades. It is by now however well recognized that peak narrowing always occur upon cooling C_{60} films or crystals, whereas the reproducibility of the energetic position of these peaks have been somewhat poorer. It has later been settled that even within an individual film, there is often a large spectral variability and accordingly, site-specific molecular packing appear to play a non-negligible role in spectral peak distribution. Even so, the C_{60} fullerene represents an archetypal molecule that always displays very characteristic molecular bond stretching vibronic features when cooled. To put the ensuing measurement of CT-state emission line-width in perspective to what is known for the temperature dependence of emission of pure organic materials,[36–38] we in Fig. 3A present the case of C_{60} photoluminescence (PL) and line-width narrowing behavior upon cooling. Fig. 3B plots the transition moment squared (determining the spectra in 3A) obtained by[39] dividing the measured spectra by E^3. This slightly altered energetic distribution properly displays the low temperature resolved vibronic progression from transitions involving at least three clearly identifiable vibrating modes. We can compare our data with the intra-molecular vibrational modes reported by

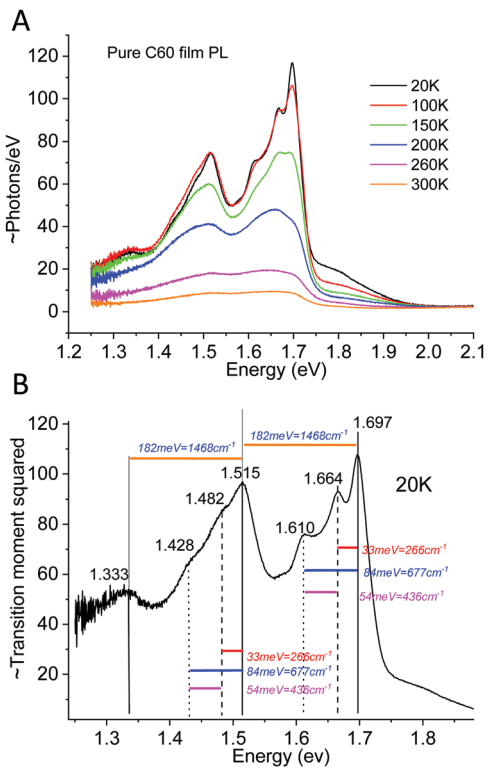

Fig. 3 (A) Temperature dependent PL emission (photon flux per eV) from pure films of C_{60}. (B) 20 K spectra divided by E^3 rendering the relevant distribution proportional to the transition moment squared. The stiff intra-molecular bond stretching completely governs the vibrational progression[35] of the spectra, whose dominant vibrational energies are designated.

Menéndez and Page[35] and conclude that the large 182 meV Ag(2) mode is easily identified. We also identify intermediate and as well as lower energy vibrational modes in the C_{60} spectra. These could be the Hg(2) and the Hg(1) mode respectively, but their values differs marginally from the stated values. The low temperature spectra in Fig. 3B accordingly shows the case of a material whose transition moment is very rich in features and shaped by both higher and lower frequency vibrational modes.

2.2. Temperature dependence of the CT-state emission line-width

Measuring the correct temperature of samples inside a cryostat may seem easy but is actually not so straightforward when the carrier concentration needs to be pronouncedly out of equilibrium to generate a detectable radiative recombination rate. Accordingly, our efforts to minimize the effects of sample Joule heating due to optical or electrical input power are summarized in the ESI.† There, we also show in Fig. S1 and S2 (ESI†) the voltage dependence of the charge-transfer state electroluminescence spectra and observe, in accordance with Gong[12] *et al.*, no noticeable peak shift with increased injection. Although these results stand as an indication that static disorder does not seem to dictate the emission, the solid proof of the pudding can only be found in detailed and accurate temperature dependent measurements of the spectral line-width.

2.2.1 Photoluminescence. Following the course of the above mentioned works, we start by showing a PL study on one complete TAPC(6%):C_{60} (6 mol% of donor) device evaluated between 20–320 K. As small molecule diluted donor cells manufactured *via* co-evaporation renders much better material intermixing compared to most efficiency optimized solution processed cells, they show PL spectra that are mostly dominated by CT-state emission. This is however generally not the case for a generic OPV cell and particularly not for the recent efficient non-fullerene acceptor based cells, where CT absorption and emission can often not be distinguished from that of pure phases.[40,41] By measuring PL on completed devices instead of merely on films on glass, it is also (often) possible to separate the CT-state emission from the excitonic emission of the pure phases in the blend. This can be achieved by evaluating the completed device under both open and shorted external circuit conditions, as outlined previously.[42] PL from pure phases in organic bulk heterojunctions originates from the recombination of strongly bound Frenkel excitons. For this type of excitons, the transition rates and emission intensity are not strongly influenced by external loading conditions. However, the emission from the CT-state, being the state responsible for the photo-voltage, is strongly effected by external loading.[42,43] Thus, by evaluating the PL emission spectra at both open circuit conditions (OC) and short circuit conditions (SC), it is possible to filter out the constant spectral contribution from the pure phases, by subtracting the PL_{SC} from the PL_{OC}. Fig. 4(A) shows the wavelength distributed PL spectra on a linear scale measured at open-circuit (solid) and short-circuit (dashed) conditions. At higher temperatures, there is a strong intensity difference between PL_{OC} and PL_{SC} (in the spectral region where CT-state emission dominates) whereas at lower temperatures, the overall intensity is stronger but the difference becomes much smaller, nonetheless remaining even at 20 K. Fig. 4B shows the normalized PL_{OC}–PL_{SC} spectra (solid) *vs.* just the normalized PL_{OC} (now dashed) spectra on a logarithmic scale. The pure phase contribution is accordingly almost fully removed in the solid curves in Fig. 4B. The remaining CT-state signal quite clearly shows a pronounced line-width narrowing as we reduce the temperature. At the lowest temperatures ($<$120 K), a further narrowing is however no longer apparent.

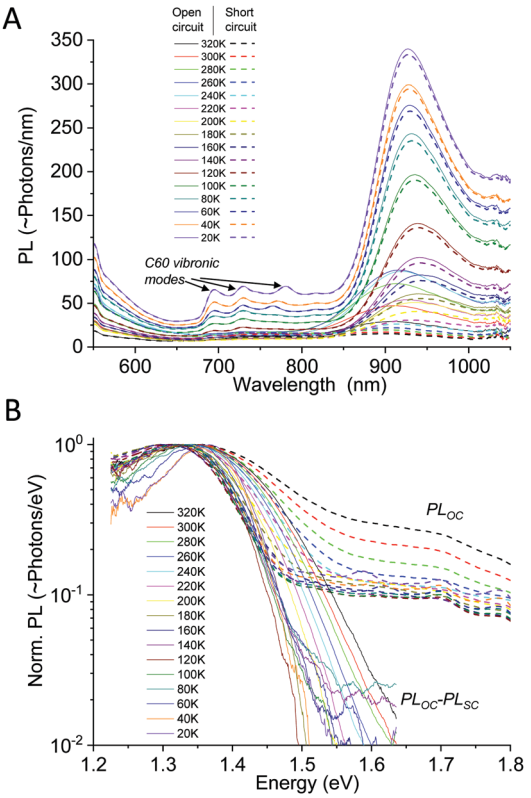

Fig. 4 (A) Photoluminescence spectra *vs.* wavelength of TAPC(6%):C_{60} measured at open and closed external circuit. Only the CT-state peak is affected by altering the external conditions. (B) Normalized PL at open circuit (dashed) *vs.* the normalized spectra obtained by subtracting the load independent pure phase emission (solid), plotted *vs.* energy. Clear line-width narrowing is observed in both the raw and the OC–SC spectra at higher temperatures, whereas a saturation appears to occur at around 120 K.

To not make any initial physical presumptions regarding the origin of the measured spectral line-width and its temperature dependence, we here first choose to fit the reduced CT-state PL spectra simply with a Gaussian distribution function:

$$\frac{\Phi(E)}{E^3} = R(E) = R_0 + A \cdot e^{-\frac{(E-E_{peak})^2}{2\sigma^2}} \quad (6)$$

with E_{peak} the energetic position of the peak and σ the standard deviation governing the spectral width. R_0 embodies the base line of the fit, which must be set quite pronounced for the pure PL_{OC} data, but can on the other hand almost be fully neglected when evaluating the PL_{OC}–PL_{SC} spectra. A spectroscopic note of high relevance for the left hand side of the equation is that the

measured photon flux $\phi(E)$ emission spectra needs to be divided by E^3, for the data to be proportional to the transition moment squared (compare the difference between Fig. 2A and B). This means in total a division of E^5 if the original measured photon flux data was distributed in wavelengths ($\sim s^{-1}$ nm^{-1}), which is most common on today's grating based spectrometers. We note that this needed correction is not always accounted for appropriately in the field of emission spectroscopy today and was also not properly accounted for in the original paper by Gould,[18] nor initially by us,[15] but has been stressed with impetus in more recent literature.[39,44]

In the classical Marcus description of CT-state emission line-widths, the variance σ^2 comprises only the dynamic contribution that corresponds to $\sigma_D{}^2 = 2kT\lambda$ (eqn (4)). The obtained Gaussian variance σ^2 of the line-width is here therefore always normalized to $2k$ and plotted in Fig. 5, which allows a direct assessment of the reorganization energy λ by simply dividing with the temperature that the spectra was measured at. The obtained values for λ are shown in the inset of Fig. 5. As the measured spectra are still not 100% perfect Gaussians, the determined variance (and λ) is to a certain extent also depending on which energy range is selected for the Gaussian fitting. An uncertainty of the variance is therefore included by evaluating a set of different energy ranges. The difficulty of correctly assigning the baseline value R_0 in eqn (6) for the PL at V_{OC} also highlights the benefit of evaluating the PL_{OC}–PL_{SC} spectra. Irrespective if we decide to evaluate the PL spectra at OC conditions (with a best attempt non-zero baseline R_0) or the PL_{OC}–PL_{SC} difference spectra, it is obvious that the variance is strongly depending on temperature for $T > 120$ K. Here, a more linearly dependent Gaussian variance on temperature (or correspondingly a more temperature independent apparent reorganization energy) indicates that thermal line-width broadening appears to be governing, at least at elevated temperatures. The observed temperature trend in CT-state PL line-width is a thus a first gauge that the classical Marcus approximation, without having to take into account static disorder, appears to be valid at higher temperatures. At lower temperatures, a saturation of the variance is however identified, and the correspondingly determined apparent reorganization energies accordingly start to increase rapidly.

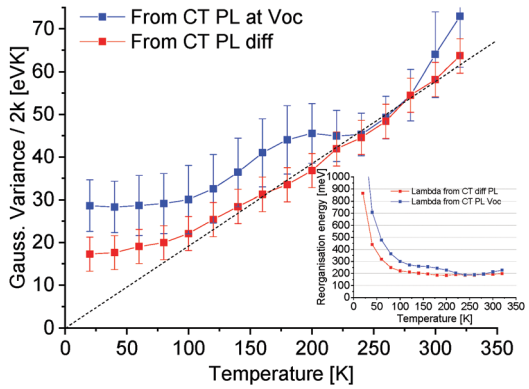

Fig. 5 Normalized variance of Gaussian fits from the TAPC(6%):C_{60} CT-state dominated emission obtained from the PL at OC or the spectra obtained from evaluating the difference between PL_{OC}–PL_{SC} as shown in Fig. 4. Inset shows the corresponding apparent reorganization energies obtained by dividing the normalized Gaussian variance by the temperature. For the subtracted spectra, a fairly constant reorganization energy is found for $T > 120$ K.

In addition to the complications of pure phase emission, a set of further concerns prevails when aiming to evaluate CT-state PL peaks, as stressed in the ESI.† Our main concern regarding CT-state PL as a probe of tail state disorder is that PL is generally not reciprocal with absorption or EQE measurements, meaning that it is not possible to relate the shape of the CT-state emission spectra to the absorption tails and *vice versa* by neither conventional van Roosbroek–Shockley[1] nor Rau's[45] electro-optical reciprocity relation. The redshifted[42] peak of CT-state EL has, on the other hand, repeatedly and unwaveringly demonstrated adherence to reciprocity[19,46] and we therefore chose to weigh our following studies on evaluating low injection electroluminescence spectra, as electrical injection better allows for population of low energy CT-states only.

2.2.2 Electroluminescence. With electroluminescence, we completely avoid population of higher energy states and a much clearer picture can immediately be offered. Fig. 6 displays the evolution of the electroluminescence spectra as a function of temperature for three small molecule and one polymer/fullerene bulk heterojunction solar cell. Three of the studied devices are co-evaporated diluted donor cells with a 6 mol% of the donor. TAPC (in A), TCTA (in B) and rubrene (in C) in C_{60} (94 mol%). The last device (in D) is a solution processed PCDTBT : PCBM70 cell in 1 : 4 stoichiometric weight-ratio. More materials studied are presented in Fig. S3 of the ESI,† together with the molecular structures of all studied materials (Fig. S4, ESI†). The devices in Fig. 6A–C are evaluated at constant current (and thus with a linearly increasing voltage with temperature to sustain the set current). To certify that our observations is not influenced by the electric field[47,48] which is determined by the applied voltage in the EL experiment, the PCDTBT:PCBM70 cell is instead shown at constant voltage, where accordingly the injection current decreases exponentially with reduced temperature. For this device, we moreover only apply 950 mV, noticeably lower than the energetic peak of emission at 1.23 eV. At this voltage, it was not possible to sustain a large enough injection current to provide any detectable emission for temperatures lower than 220 K (where merely 311 μA cm^{-2} was injected).

The benefit of EL as compared to PL is very obvious. As all electroluminescence spectra are now entirely dominated by interfacial low energy CT-state radiative recombination, we can easily cover a CT-state intensity range of 3–4 decades. All devices show a very broad EL-spectra apart from the rubrene:C_{60} device, which is noticeably narrower. For all devices, independent of being evaluated under constant current or constant voltage mode, we observe a substantial narrowing of the CT-state EL spectra upon cooling.

With EL allowing access to a larger logarithmic intensity range, a superior approach, compared to Gaussian functional fitting (as implemented above for PL) becomes straightforwardly available to determine the correct value of the Gaussian variance. If the line-shape is perfectly Gaussian, the first derivative of $\ln(\phi(E)/E^3)$

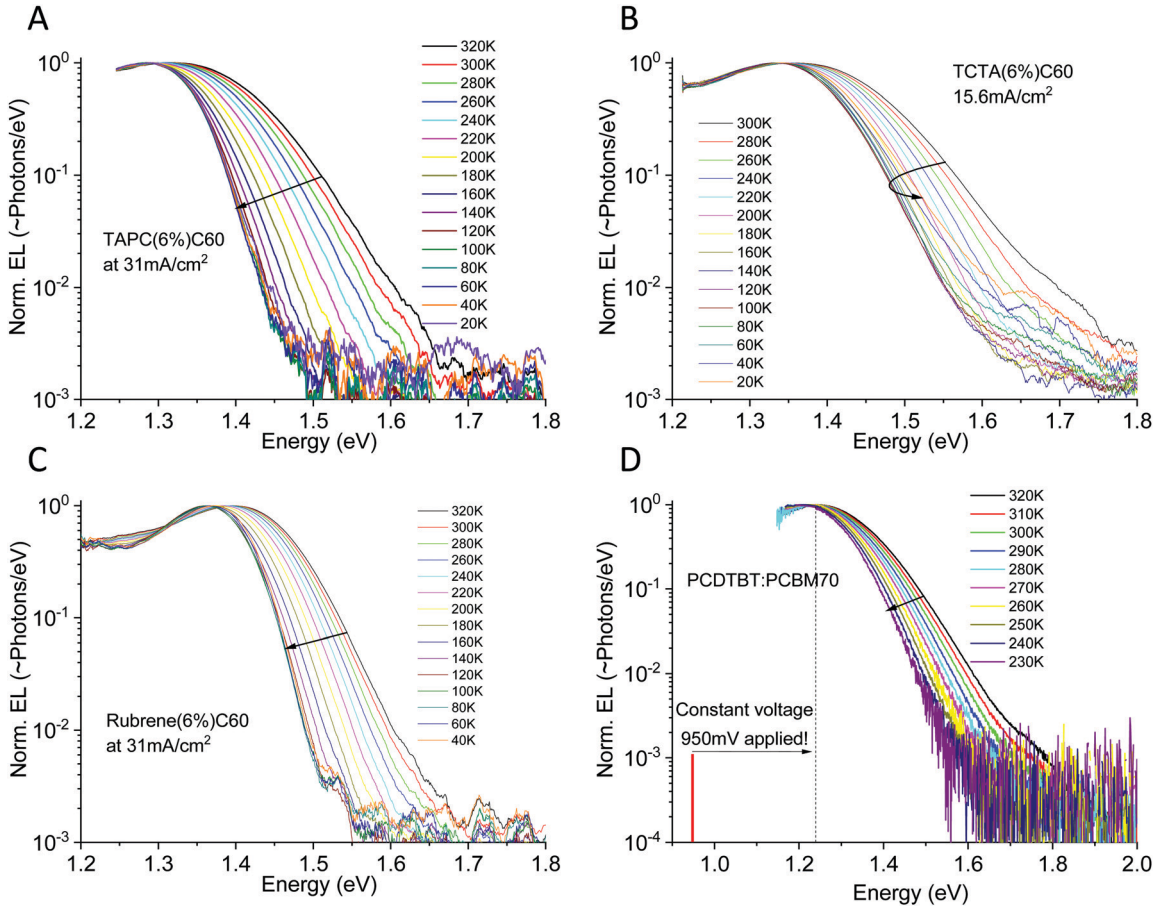

Fig. 6 Electroluminescence spectra *vs.* temperature for four different organic solar cells. (A), (B) and (C) shows small molecule diluted donor devices based on TAPC:C_{60}, TCTA:C_{60} and rubrene:C_{60} run at constant current, whereas (D) shows a polymer PCDTBT:PCBM70 device instead evaluated at constant voltage. All devices show noticeable CT-state line-width narrowing as well as a small, but detectable, EL peak red-shift upon cooling. More materials studied are presented in the ESI,† in Fig. S3.

is equal to $-(E - E_{peak})/\sigma^2$ and the second derivative equates the inverse of the variance and is consequently a constant, fully independent of E;

$$\sigma^2 = -\frac{1}{\frac{d^2\left(\ln\left(\frac{\Phi(E)}{E^3}\right)\right)}{dE^2}} \quad (7)$$

However, as the second derivatives of measured experimental data (even EL) are easily getting markedly noisy, we here stay with evaluating the inverse slope of the first derivate of the logarithmic data, as outlined in Fig. 7 for TAPC(6%) and the rubrene(6%) devices.

The straight lines covering a few hundreds of millivolts first quite clearly confirm that a majority of the measured line-shapes indeed are of true Gaussian shape. The lowest temperature data however also start to display noticeable deviations from linearity, as the line-widths are here no longer truly Gaussians (*vide infra*). The data in Fig. 6 and 7 accordingly provides the most decisive experimental quantification of the true CT-state line-width dependency on temperature. Following this method for the EL spectra of the other devices, allows us to in Fig. 8A present the $2k$ normalized variance from all evaluated data, together with the results previously found by Kahle *et al.* and Burke *et al.* Fig. 8B shows the corresponding total (or "apparent"[21]) reorganization energies (λ). From the EL data we can now clearly confirm a variance which is quite linear with temperature for $T > 120$ K for the TAPC and rubrene devices. The TCTA cell shows instead what seems to comprise two different linear regions, with a bending point at $\sim$200 K. At lower temperatures, a saturation of the variance is again clearly identified in all three samples, and the correspondingly determined apparent reorganization energies accordingly start to increase rapidly. We remind the reader though at these lowest temperatures the variance is no longer truly Gaussian. The observed high temperature trend in CT-state EL line-width thus appears to corroborate the classical Marcus approximation, without having to account for any noticeable static disorder, whereas the low temperature saturated line-width data implies something else. The pronounced line-width narrowing upon cooling is thus in quite strong experimental contrast to the recent observations by Kahle *et al.*, Burke *et al.* and earlier Jarzab *et al.* These prior works observed no significant CT-state line-width narrowing, and thus concluded that static disorder contribution is strongly dictating the spectra

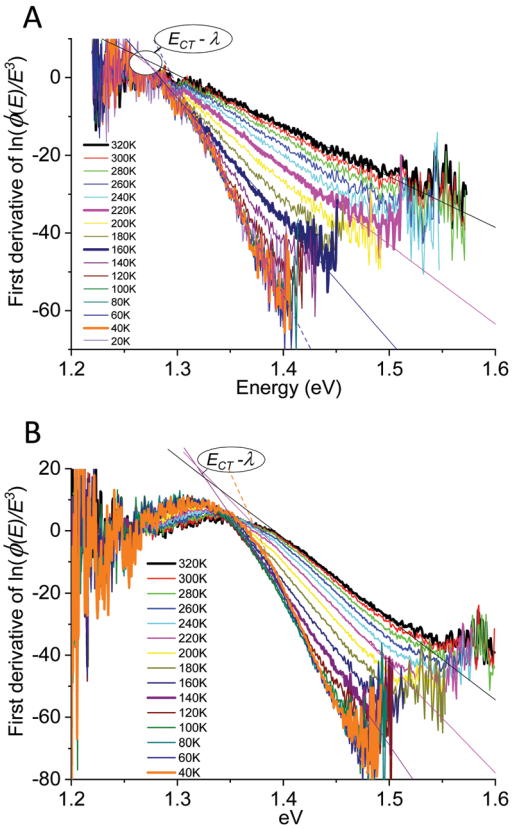

Fig. 7 Measured temperature-dependent variance of the (A) TAPC(6%)C_{60} and (B) rubrene(6%)C_{60} spectra as determined from the first derivative of $\ln(\phi(E)/E^3)$. A majority of the data are straight lines and thus allows to confirm both a Gaussian line-shape as well as to determine the Gaussian variance value from the inverse of the slope, confirmed as being strongly temperature dependent. The highlighted converging point correspond to the peak of emission being equal to $E_{CT} - \lambda$. We also here note that the lowest temperature data shows clear deviation from linearity confirming that they did not originated from a perfectly Gaussian line-shape.

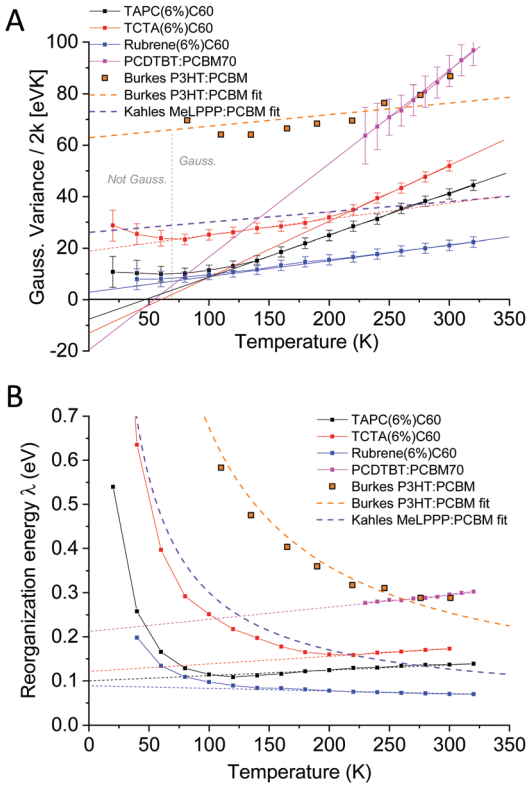

Fig. 8 (A) Temperature dependence of the obtained Gaussian variance of the E^3 reduced spectra from the electroluminescence in Fig. 6. (B) The corresponding ("apparent") reorganization energy, determined by dividing the data in (A) with the temperature. Whereas Burke's EQE and Kahle's PL data showed strongly T-dependent reorganization energies (almost constant variance dominated by static disorder) our data do not indicate any pronounced contribution to line-width broadening from static disorder.

(orange and purple dashed lines in graph). From our data, we note instead that when extrapolating the linear variance from the high temperature regime towards zero Kelvin, we are in fact not able to confirm any pronounced positive deviation from zero. According to eqn (3), this shows that the static disorder broadening does not seem to be of any significance to the measured line-width, at least in our fairly large set of evaluated samples. What is however also evident from Fig. 8A is the apparent negative values obtained when extrapolating the high temperature linear variance regime towards zero Kelvin, particularly perceptible for the TAPC and TCTA data (PCDTBT having a larger error margin). Having re-measured these spectra and re-evaluated the data carefully it is clear that this is not within the experimental error-margin, and truly that "negative static disorder" would be implied for those materials. This, at first highly puzzling observation, does therefore not at all seem to fit with the prior description of the simple summation of a static and a dynamic variance as suggested previously[21] and offered above in eqn (3). As also the clearly observed saturation of the line-width variance at lower temperatures is not possible to reconcile with neither classical Marcus nor the simple summation of the two disorder contributions, we here therefore judge that a F–C treatment beyond the classical Marcus picture is utterly necessary. Below, we show that both the line-width saturation at low temperatures as well as the negative extrapolated values at zero K, from the high temperature regime, are indeed present in a full F–C treatment.

2.3. Theory on line-width saturation and Keil's equation

In a full quantum mechanical treatment, the impact of harmonic vibrations with characteristic energy $\hbar\omega$ on the emission spectrum is reflected in the following complete Franck–Condon formula:[49,50]

$$\phi(E) \sim E^3 \sum_i \sum_j \langle \nu_i | \nu_j \rangle^2 \mathrm{LW}(E + i\hbar\omega - (E_G + j\hbar\omega)) \mathrm{e}^{-\frac{j\hbar\omega}{kT}} \tag{8}$$

Herein is $\langle \nu_i | \nu_j \rangle$ the overlap integral between the i:th ground state vibrational level and j:th excited state vibrational level and LW is a function expressing the line-width of the individual transitions between any excited and ground state vibrational level. In the absence of other sources of disorder, LW is represented by a delta-function. For an harmonic oscillator[50,51]

$$\langle \nu_i | \nu_j \rangle^2 = \mathrm{e}^{-s} S^{(j-i)} \frac{i!}{j!} \left(L_i^{(j-i)}(S) \right)^2 \tag{9}$$

With $L_n^{\alpha}(x)$ the Laguerre polynomial and S the Huang–Rhys factor being equal to $\lambda/\hbar\omega$. With the help of computer code, we can now evaluate the emission spectra according to eqn (8) and (9), where two limiting cases deserve our detailed attention. We will first evaluate the case when the vibrational spacing $\hbar\omega$ is relatively small and S is moderately large. In this limit, the spectral shape of $\phi(E)/E^3$ approaches a Gaussian line-shape at elevated temperatures.

As outlined above in the analysis of the experimental data in Fig. 7, if the line-shape is perfectly Gaussian, the first derivative of the logarithm of the data should be a straight line. For the calculated high temperature curves in Fig. 9A and B, with $S = 10$ and $\hbar\omega = 15$ meV, this is indeed the case. However, at the lowest temperatures the line-shape deviates considerably from Gaussian and assumes instead the so-called Pekarian shape. For all temperatures, the second derivative is evaluated at $E - E_{gap} = 0$ and is plotted as a function of temperature in Fig. 9C. As can be seen the obtained temperature dependence of both the first derivative and the variance display quite the same behavior as the measured ones presented in Fig. 7 and 8.

As the variance shows a saturation at low temperature and a linear behavior at higher temperatures, its behavior corresponds rather well with the semi-classical formula for the variance σ_D^2 of the line-shape as derived in the 1965 seminal work (eqn (3.11)) by Thomas Keil:[51]

$$\sigma_D^2 = \lambda\hbar\omega \cdot \coth\left(\frac{\hbar\omega}{2kT}\right) \quad (10)$$

In this expression, outlined as the solid thick blue line in Fig. 9C for $S = 10$ and $\hbar\omega = 15$ meV, we note again that at lower temperatures the dynamic variance σ_D becomes constant, and the constant value equates $\lambda\hbar\omega$ while at sufficiently high temperature it is instead proportional to T, recovering the classical Marcus variance $2\lambda kT$. Keil's expression therefore nicely embodies the general behavior of line-width narrowing, but can, in the low temperature regime, unfortunately not be used directly to with accuracy assign the correct vibrational energy and Huang–Rhys factor, as seen in Fig. 9C. What can however be concluded from the above modelling is that low energy vibrations ($\hbar\omega <$ 20 meV) and moderately large Huang–Rhys factors can describe the overall temperature behavior of the CT-state line-width, without having to invoke static disorder.

Fig. 10 sketches the corresponding potential energy configuration coordinate diagram for the ground and excited state for such a modeled system with moderately large Huang–Rhys factors (and thus a large reorganization energy (λ) in combination with small vibrational (densely spaced) energy levels ($\hbar\omega$)).

As our data are in quite decent agreement with Keil's equation, with an almost constant non-zero line-width observed at lower temperatures (<120 K), we therefore argue that the spectral line-width of the CT-state emission should be treated as experiencing a transition from the classical high temperature Marcus regime, where several of the higher vibronic levels of the exited state are thermally populated (Fig. 10A), to a low temperature regime where only the lowest vibrational level of the excited state is populated (Fig. 10B). When reducing the temperature further, no more narrowing is possible as no further reduction of populated vibrational energy levels of the excited state can occur. The constant line-width (given by $\lambda\hbar\omega$), is then governed only by the shape of the potential energy parabola according to Keil's equation. The two resulting line-width equations are inserted for the two limiting cases presented in panel (A) and (B) of Fig. 10. A linear temperature dependence at elevated temperatures therefore suggest that the classical Marcus approximation implemented previously (at high temperatures) is well justified for bulk heterojunction solar cells whose transitions are governed by interfacial CT-states, whereas Keil's semi-classical equation outlines better what takes place in the entire temperature range.

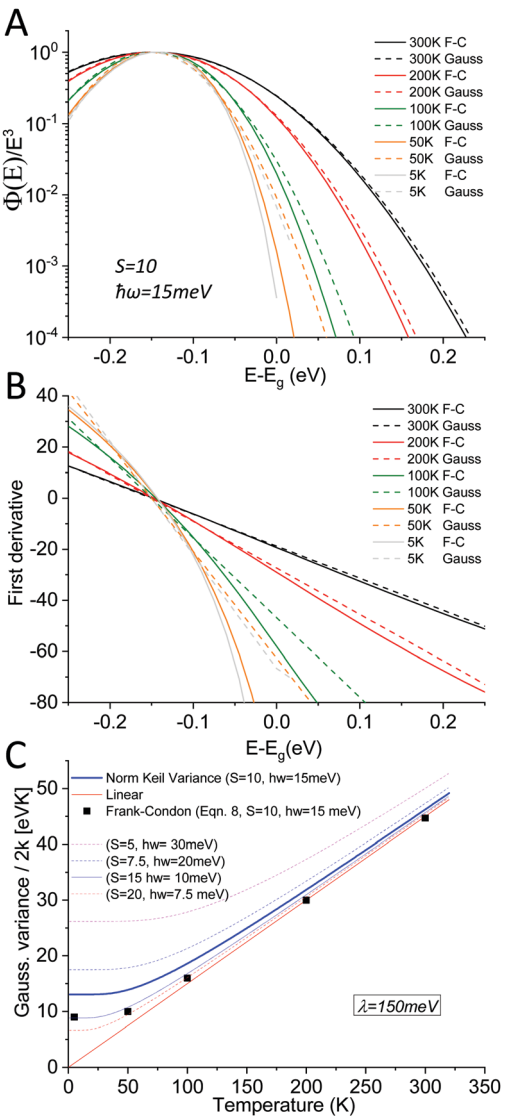

Fig. 9 (A) shows eqn (8) plotted for $S = 10$, $\hbar\omega = 15$ meV ($\lambda = 150$ meV) at a set of selected temperatures. The dashed lines are Gaussians with their variance given by the Keil equation (eqn (9)). (B) shows the first derivate of the logarithm of the data in (A). The high temperatures are nicely represented by Gaussians (straight lines) whereas it is clear that the low T data are not. Note the similarity to the derivative of the experimental data in Fig. 7. (C) shows the corresponding variance from the calculated spectra, as obtained *via* eqn (8) as well as from the semi-classical Keil equation (eqn (10)).

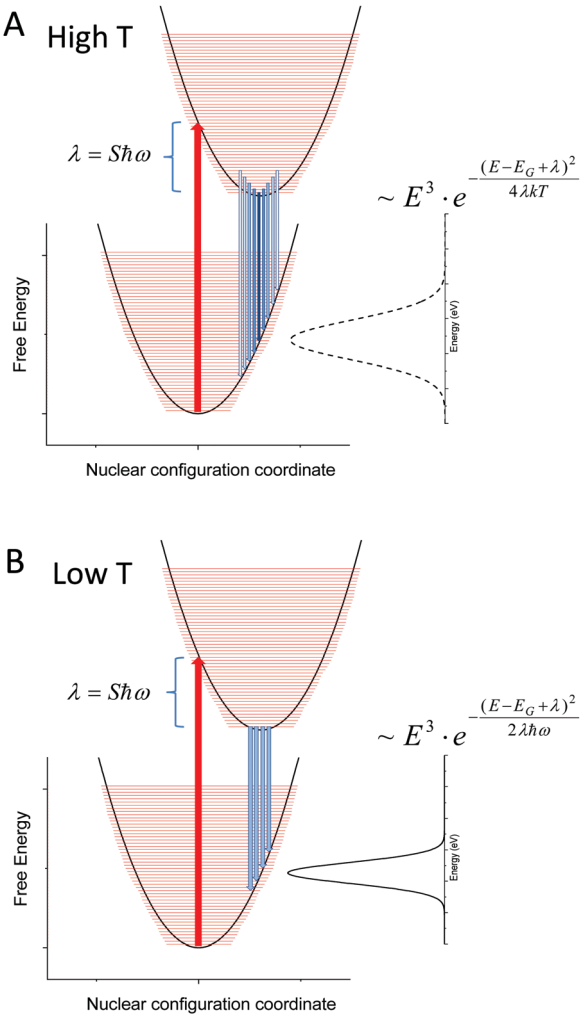

Fig. 10 (A) Outlines the population at higher T (120–320 K) of a material with densely spaced vibronic energies and a corresponding large Huang–Rhys factor as measured in our set of samples. The linewidth of the unstructured emission spectra is broadened with increasing temperature and the classical Marcus expression is justified. In (B), only the lowest vibrational level of the exited state is populated and the corresponding variance of the (still unstructured) emission spectra is constant and defined by the product of reorganization energy and the vibronic spacing.

The classical approximation stipulates that the relevant vibronic energy levels are so densely spaced, that there is no argument for invoking the quantum mechanical description for the high-energy part of the emission tails at room temperature. The question to resolve is consequently; how to justify the observed presence of such small and densely spaced vibronic energy levels also in the solid state? Bearing in mind that the CT emission in OPV blends is per definition occurring at the interface between (rather large) molecules, it is well justified to assume that the intermolecular motions should play a more dominant role, and not only the intra-molecular (C–C, C–H) high-energy modes of the molecules themselves. Merely the motion of extended parts of the molecules may be dominating the low frequency interface interactions. These may comprise extremities such as single bond attached rings present in most of our studied small molecules, or even just sidechains as present in the soluble polymers. Accordingly, at higher temperatures, the thermal energy of a system ruled by interface interaction can be considered high with respect to the low frequency vibrations originating from these slow and small movements that appears to govern the CT-state spectra, and the classical approximation accordingly becomes justified. This picture might however be less valid for significantly stiffer molecules, such as the MeLPPP combined with $PCBM_{60}$, which *e.g.* Kahle *et al.* focused on.

The observed transition of spectral line-width from a low temperature constant value to a temperature dependent line-width at higher temperatures, along with Keil's equation, has in fact been identified several times throughout the history of material spectroscopy, and for vastly different materials. Meyer,[52] Dexter,[53] Toyozawa,[54] Keil,[55] Mahr[56] and Kurik[2,57] have all confirmed the above observed temperature behavior, but in completely different materials, and often with an exponential tail instead of a Gaussian. Recalling the Urbach tail introduction of the manuscript, we here therefore also stress the almost identical expression as Keil's equation, frequently found for the temperature dependence of the exponential tail slope; namely the dynamic part of the Urbach energy.[2,57]

$$E_{\mathrm{U,Dyn}}(T) = \frac{\hbar\omega}{2\sigma_0} \cdot \coth\left(\frac{\hbar\omega}{2kT}\right) \tag{11}$$

In this expression, all features of temperature dependence is identical as in Keil's semi-classical expression. The only differing term is found in the pre-factor σ_0, specified in ref. 57, which from by comparison to Keil, should correspond to the inverse of the reorganization energy λ.

2.4. Explanation of negative extrapolated variance values; a multimode analysis

Having first settled the occurrence of line-width saturation at low temperatures with Keil's semi-classical description, we also need to understand the perplexing observation of the 0 K extrapolated negative linewidth values in Fig. 8A. An explanation for this is found in the fact that in real systems, multiple vibrational modes with different energies are expected to be present. Let us therefore now consider the simplest case where one high and one low frequency mode are present simultaneously. As shown above, the low frequency modes are responsible for a Gaussian like line-width. Including high frequency modes can be done by again using the general eqn (8). This time we however let $\langle \nu_i | \nu_j \rangle$ represent the overlap integral between the i:th ground state vibrational level and the j:th excited state vibration level of a high frequency mode. In this example, presented in Fig. 11A, we take this high frequency mode to have a large value $\hbar\omega$ = 0.15 eV, and a typical low value of the Huang–Rhys factor S = 1, representative for a classic C–C vibration (as also seen to dominate the pure fullerene case of Fig. 3). The LW function is this time taken to instead be a Gaussian with its line-width determined by the Keil formula (eqn (10)) with the S and $\hbar\omega$ parameters of a low frequency mode. The low frequency mode is, as above, taken to be $\hbar\omega$ = 0.015 eV and with S = 10. This parameter selection leads to emission spectra peaking at a value of 150 meV below E_{gap}. In a

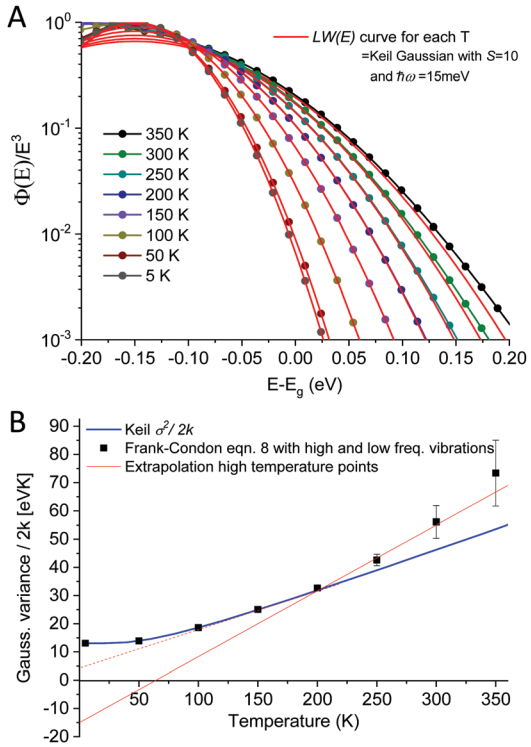

Fig. 11 (A) shows eqn (8) now accounting for both high and low frequency vibrational modes. The red lines represents the line-width associated with only the low frequency modes, whose behavior is now set to be defined by Keil's equation. (B) shows the corresponding calculated normalized Gaussian variance, as determined from the second derivative. At low temperatures the variance is governed by the low frequency modes, whereas at higher temperatures also the high frequency mode is populated, further broadening the spectra (and increasing the variance).

classical picture, a single reorganization energy of 150 meV would thus be assigned if a single measurement at room temperature would be performed. The LW function as well as the full Frank–Condon expression, according to eqn (8), is therefore again plotted for several temperatures in the figure, allowing us to discriminate the influence of both modes.

One sees that at low T, the full expression (8) is almost identical to the low frequency mode LW function. At high T however, higher energy vibrational states of the high frequency mode start to become populated, leading to an additional steeper broadening with T. When again determining σ^2 from the second derivative approach as outlined above, we obtain the line-widths with associated variance as presented in Fig. 11B and once more confirm that at low T, the line-width equals that of the low frequency mode. At higher temperatures, the line-width broadens further, due to additional thermal population of the high frequency modes. We therefore argue that Fig. 11 may very well represent the theoretical case of the experimental measurements, of for example the TCTA(6%):C_{60} device, which showed similar behavior and is thus expected to have pronounced influence of both high and low vibrational modes. We believe that also the other devices that too showed negative extrapolation therefore likely are governed by combinations of different energy modes. Although rubrene is the only material that appears to indicate a (very small) positive static disorder in Fig. 8b, we want to emphasize that, as its low frequency reorganization energy is much smaller than the other materials, one would have to measure emission with even higher sensitivity to detect the effect of the present high frequency modes. Accordingly, our work strongly supports the theoretical approach taken by Kahle *et al.*, arguing that a complete Frank–Condon picture is indeed needed to account for the entire temperature dependence of the CT-state line-width. Our experimental observations on the other hand do not corroborate Kahle's claim on the strong influence of static disorder. We finally note the very recent manuscript by Linderl *et al.*,[58] who observed a very similar behavior in DBP:C_{60} devices as we have done herein.

3. Conclusions

The broad room temperature spectral line-width of interfacial charge-transfer-state emission of organic solar cells does not appear to be an effect of energetic static disorder. Instead, the larger part of the line-width at 300 K is originating from thermally activated molecular motion, which can be quite well described by the reorganization energy in the classical Marcus formalism. The spectral line-width of CT-state transitions at room temperature is thus mainly broadened by strong coupling to molecular vibrations, and not by static disorder broadening. Our conclusion on these matters is based on a very strong experimental observable; the emission line-width at high temperatures is a linear function that does not extrapolate to noticeable positive values at zero Kelvin. At lower temperatures, we however clearly observe a saturation of the line-width and thus a breakdown of the classical Marcus picture. Below this temperature, the line-width is no longer broadened by recombination from higher vibronic levels of the excited state, but instead more ruled by the shape of the potential parabola of the harmonic oscillator. A full quantum mechanical treatment is in line with Thomas Keil's semi-classical expression of line-width broadening as presented in eqn (10), bearing a strong similarity to the dynamic Urbach tail expressions.[2] From this, we conclude that low energy vibrations in combination with moderately large Huang–Rhys factors are most likely responsible for the observed temperature dependence of the line-width broadening. To be able to fully reconcile the sometimes-steeper temperature dependence at higher temperatures, we also outlined the inclusion of simultaneous low and high energy vibrational contribution in a Frank–Condon framework. Considering our observations on overall vibrational dominance to the emission line-width and accordingly to the, from reciprocity relations corresponding, absorption tail, we conclude that any Gaussian disorder parameters (or equivalent exponential Urbach energies) obtained from pure optical measurements is unlikely to be directly defined by only the tail shape of a static DOS of the material blend. As such, any static disorder parameter linked to the DOS shape cannot be determined from single temperature absorption tail measurements. As a final concluding note on this matter, we would also like to make it clear that although we

cannot find any evidence of discernable static disorder contribution to CT-state emission broadening, we do not want to argue that static disorder is not present in organic semiconductors, as our data provides no evidence for such a more general statement. It is still very possible that tail states that are not associated with an optical transition moment (oscillator) are still present. As these dark states do not couple to absorption or emission events, they do not affect the measurements performed herein but would still be able to play a role in the transport of charge carriers.

Author contribution

J. B. manufactured the small molecules co-evaporated diluted donor cells in Dresden. K. T. manufactured the solution processed polymer devices in Würzburg. K. T. measured the *T*-dependent EL and PL spectra and the corresponding *L–I–V* curves of all devices in Würzburg. All authors analyzed the data (multiple times) and discussed the results. K. V. conducted the Franck–Condon calculations. K. T. wrote the paper, to which K. V. and J. B. provided feedback and amendments. The study was designed collectively by all authors.

Conflicts of interest

There are no conflict to declare.

Acknowledgements

K. T. acknowledges the German Research Foundation (DFG) through project 382633022 (RECOLPER) and the Experimental Physics VI chair of Prof. Vladimir Dyakonov at Würzburg University. J. B. acknowledges the DFG project VA 1035/5-1 (Photogen) and the Sächsische Aufbaubank through project no. 100325708 (Infrakart). The authors also acknowledge discussion on the topic with Robert Street, Thomas Kirchartz, Frank Ortmann and Carsten Deibel.

Notes and references

1 W. van Roosbroeck and W. Shockley, *Phys. Rev.*, 1954, **94**, 1558.
2 I. Studenyak, M. Kranjcec and M. Kurik, *Int. J. Opt.*, 2014, **4**, 76–83.
3 D. Redfield, *Phys. Rev.*, 1963, **130**, 916.
4 T. Tiedje, B. Abeles and J. M. Cebulka, *Solid State Commun.*, 1983, **47**, 493–496.
5 H. Oheda, *Jpn. J. Appl. Phys.*, 1979, **18**, 1973–1978.
6 G. D. Cody, T. Tiedje, B. Abeles, B. Brooks and Y. Goldstein, *Phys. Rev. Lett.*, 1981, **47**, 1480–1483.
7 F. Urbach, *Phys. Rev.*, 1953, **92**, 1324.
8 C. W. Greeff and H. R. Glyde, *Phys. Rev. B: Condens. Matter Mater. Phys.*, 1995, **51**, 1778–1783.
9 R. A. Street, K. W. Song, J. E. Northrup and S. Cowan, *Phys. Rev. B: Condens. Matter Mater. Phys.*, 2011, **83**, 165207.
10 B. E. Pieters, T. Kirchartz, T. Merdzhanova and R. Carius, *Sol. Energy Mater. Sol. Cells*, 2010, **94**, 1851–1854.
11 J. Krustok, H. Collan, M. Yakushev and K. Hjelt, *Phys. Scr., T*, 1999, **79**, 179–182.
12 W. Gong, M. A. Faist, N. J. Ekins-Daukes, Z. Xu, D. D. C. Bradley, J. Nelson and T. Kirchartz, *Phys. Rev. B: Condens. Matter Mater. Phys.*, 2012, **86**, 024201.
13 U. Hörmann, S. Zeiske, S. Park, T. Schultz, S. Kickhofel, U. Scherf, S. Blumstengel, N. Koch and D. Neher, *Appl. Phys. Lett.*, 2019, **114**, 183301.
14 U. Hörmann, S. Zeiske, F. Piersimoni, L. Hoffmann, R. Schlesinger, N. Koch, T. Riedl, D. Andrienko and D. Neher, *Phys. Rev. B*, 2018, **98**, 155312.
15 K. Vandewal, K. Tvingstedt, A. Gadisa, O. Inganäs and J. V. Manca, *Phys. Rev. B: Condens. Matter Mater. Phys.*, 2010, **81**, 125204.
16 R. S. Crandall, *Phys. Rev. Lett.*, 1980, **44**, 749–752.
17 R. A. Marcus, *J. Chem. Phys.*, 1956, **24**, 966–978.
18 I. R. Gould, D. Noukakis, L. Gomezjahn, R. H. Young, J. L. Goodman and S. Farid, *Chem. Phys.*, 1993, **176**, 439–456.
19 K. Vandewal, K. Tvingstedt, A. Gadisa, O. Inganäs and J. V. Manca, *Phys. Rev. B: Condens. Matter Mater. Phys.*, 2010, **81**, 125204.
20 K. Vandewal, K. Tvingstedt and O. Inganäs, *Semiconductors and Semimetals*, Elsevier, 2011, vol. 85, pp. 261–295.
21 T. M. Burke, S. Sweetnam, K. Vandewal and M. D. McGehee, *Adv. Energy Mater.*, 2015, **5**, 1500123.
22 V. Coropceanu, J. Cornil, D. A. da Silva, Y. Olivier, R. Silbey and J. L. Bredas, *Chem. Rev.*, 2007, **107**, 926–952.
23 K. Vandewal, J. Benduhn, K. S. Schellhammer, T. Vangerven, J. E. Ruckert, F. Piersimoni, R. Scholz, O. Zeika, Y. L. Fan, S. Barlow, D. Neher, S. R. Marder, J. Manca, D. Spoltore, G. Cuniberti and F. Ortmann, *J. Am. Chem. Soc.*, 2017, **139**, 1699–1704.
24 F. J. Kahle, A. Rudnick, H. Bässler and A. Köhler, *Mater. Horiz.*, 2018, **5**, 837–848.
25 J. Jortner, *J. Chem. Phys.*, 1976, **64**, 4860–4867.
26 D. Jarzab, F. Cordella, J. Gao, M. Scharber, H. J. Egelhaaf and M. A. Loi, *Adv. Energy Mater.*, 2011, **1**, 604–609.
27 I. Riisness and M. J. Gordon, *Appl. Phys. Lett.*, 2013, **102**, 113302.
28 M. List, T. Sarkar, P. Perkhun, J. Ackermann, C. Luo and U. Wurfel, *Nat. Commun.*, 2018, **9**, 3631.
29 Z. Vaitonis, P. Vitta and A. Zukauskas, *J. Appl. Phys.*, 2008, **103**, 093110.
30 E. F. Schubert, *Light-Emitting Diodes*, Cambridge University Press, 2nd edn, 2006.
31 H. W. Kroto, J. R. Heath, S. C. O'Brian, R. F. Curl and R. E. Smalley, *Nature*, 1985, **318**, 162.
32 P. M. Pippenger, R. D. Averitt, V. O. Papanyan, P. Nordlander and N. J. Halas, *J. Phys. Chem.*, 1996, **100**, 2854–2861.
33 E. J. Shin, J. H. Park, M. Y. Lee, D. H. Kim, Y. D. Suh, S. I. Yang, S. M. Jin and S. K. Kim, *Chem. Phys. Lett.*, 1993, **209**, 427–433.
34 V. Capozzi, M. Santoro, G. Perna, G. Celentano, A. Minafra and G. Casamassima, *Eur. Phys. J.: Appl. Phys.*, 2001, **14**, 3–11.
35 J. Menéndez and J. B. Page, Vibrational spectroscopy of C_{60}, in *Light Scattering in Solids VIII. Fullerenes, Semiconductor Surfaces, Coherent Phonons*, ed. M. Cardona and G. Güntherodt, Topics in Applied Physics, Springer, Berlin, Heidelberg, 2006, vol. 76, pp. 27–95.

36 P. J. Brown, D. S. Thomas, A. Köhler, J. S. Wilson, J. S. Kim, C. M. Ramsdale, H. Sirringhaus and R. H. Friend, *Phys. Rev. B: Condens. Matter Mater. Phys.*, 2003, **67**, 064203.
37 S. Guha, J. D. Rice, Y. T. Yau, C. M. Martin, M. Chandrasekhar, H. R. Chandrasekhar, R. Guentner, P. S. de Freitas and U. Scherf, *Phys. Rev. B: Condens. Matter Mater. Phys.*, 2003, **67**, 125204.
38 S. T. Hoffmann, H. Bässler and A. Köhler, *J. Phys. Chem. B*, 2010, **114**, 17037–17048.
39 J. Mooney and P. Kambhampati, *J. Phys. Chem. Lett.*, 2013, **4**, 3316–3318.
40 S. S. Chen, Y. M. Wang, L. Zhang, J. B. Zhao, Y. Z. Chen, D. L. Zhu, H. T. Yao, G. Y. Zhang, W. Ma, R. H. Friend, P. C. Y. Chow, F. Gao and H. Yan, *Adv. Mater.*, 2018, **30**, 1804215.
41 L. Perdigon-Toro, H. T. Zhang, A. S. Markina, J. Yuan, S. M. Hosseini, C. M. Wolff, G. Z. Zuo, M. Stolterfoht, Y. P. Zou, F. Gao, D. Andrienko, S. Shoaee and D. Neher, *Adv. Mater.*, 2020, **32**, 1906763.
42 K. Tvingstedt, K. Vandewal, F. Zhang and O. Inganäs, *J. Phys. Chem. C*, 2010, **114**, 21824–21832.
43 K. Tvingstedt, O. Malinkiewicz, A. Baumann, C. Deibel, H. J. Snaith, V. Dyakonov and H. J. Bolink, *Sci. Rep.*, 2014, **4**, 6071.
44 M. de Jong, L. Seijo, A. Meijerink and F. T. Rabouw, *Phys. Chem. Chem. Phys.*, 2015, **17**, 16959–16969.
45 U. Rau, *Phys. Rev. B: Condens. Matter Mater. Phys.*, 2007, **76**, 085303.
46 K. Vandewal, K. Tvingstedt, A. Gadisa, O. Inganäs and J. V. Manca, *Nat. Mater.*, 2009, **8**, 904–909.
47 W. Franz, *Z. Naturforsch., A: Phys. Sci.*, 1958, **13**, 484–489.
48 R. Williams, *Phys. Rev.*, 1962, **126**, 442.
49 P. K. H. Ho, J. S. Kim, N. Tessler and R. H. Friend, *J. Chem. Phys.*, 2001, **115**, 2709–2720.
50 M. Malagoli, V. Coropceanu, D. A. da Silva and J. L. Bredas, *J. Chem. Phys.*, 2004, **120**, 7490–7496.
51 T. H. Keil, *Phys. Rev.*, 1965, **140**, A601.
52 H. J. G. Meyer, *Physica*, 1954, **20**, 1016–1020.
53 D. L. Dexter, *Nuovo Cimento, Suppl.*, 1958, **7**, 245–286.
54 Y. Toyozawa, *Prog. Theor. Phys.*, 1959, **22**, 455–457.
55 T. H. Keil, *Phys. Rev.*, 1966, **144**, 582.
56 H. Mahr, *Phys. Rev.*, 1963, **132**, 1880.
57 M. V. Kurik, *Phys. Status Solidi A*, 1971, **8**, 9.
58 T. Linderl, T. Zechel, A. Hofmann, T. Sato, K. Shimizu, H. Ishii and W. Brütting, *Phys. Rev. Appl.*, 2020, **13**, 024061.

